Nanotechnology **19** (2008) 095705 (8pp) doi:10.1088/0957-4484/19/9/095705

Fabrication of a multi-scale nanostructure of TiO_2 for application in dye-sensitized solar cells

Cheng-Yu Kuo and Shih-Yuan Lu

Department of Chemical Engineering, National Tsing-Hua University, Hsinchu, Taiwan 30043, Republic of China

E-mail: sylu@mx.nthu.edu.tw

Received 14 October 2007, in final form 12 December 2007
Published 12 February 2008
Online at stacks.iop.org/Nano/19/095705

Abstract

We propose a highly ordered multi-scale nanostructure of TiO_2 for applications as an anode in dye-sensitized solar cells (DSSCs). The structure is composed of a TiO_2 blocking layer, a TiO_2 inverse opal main body, regularly arranged transport channels between contacting spherical voids of the TiO_2 inverse opal, and TiO_2 nanoparticles coated on the spherical surfaces of the voids. The ordered and continuous backbone of the inverse opal serves as the fast electron transport pathways while the regularly arranged transport channels enable easy transport of dye and electrolyte within the structure. A multi-cycle procedure was developed to enable fabrication of thick inverse opals and easy adjustment of the inverse opal thickness. An example structure was constructed, involving a blocking layer of 90 nm thickness, an inverse opal of 100 nm voids, transport channels of 30–50 nm openings, and nanoparticles 10–15 nm in size. An open-circuit voltage decay investigation showed a significant improvement in electron lifetime for the proposed multi-scale TiO_2 nanostructure based DSSC than that of a TiO_2 nanoparticle film based DSSC, revealing the superior electron recombination characteristic offered by the proposed TiO_2 nanostructure. The conversion efficiency of the DSSC assembled from such an anode structure can reach 4% with a short-circuit current density (J_{sc}) of 8.7 mA cm^{-2} and open-circuit potential (V_{oc}) of 0.76 V under AM 1.5 (100 mW cm^{-2}) illumination.

1. Introduction

Since the pioneering work of O'Regan and Grätzel [1] in 1991 demonstrating the great potential of dye-sensitized solar cells (DSSCs) as an inexpensive alternative to conventional silicon based solar cells, extensive and intensive continuing research efforts have been conducted to further the development of DSSCs [2–10]. A typical DSSC is composed of four main units: the inorganic porous film, dye, electrolyte, and counter electrode. The inorganic porous film, typically constructed from casting TiO_2 nanoparticles (NPs) on a transparent conducting glass, e.g., glass coated with a thin layer of fluorine doped tin oxide (FTO), serves as the anode of the DSSC. This TiO_2 porous film, with a typical thickness of 10–15 μm, is sensitized with adsorbed dye to harvest light and generate and conduct photocurrents. The electrolyte, containing a redox couple I_3^-/I^- mediator, is injected into the gap between the anode and the catalytic Pt counter electrode. As the dye absorbs the incident sunlight of proper wavelengths, electron–hole pairs are generated and the electrons are injected into the TiO_2 porous film, transported to and collected at the FTO layer, and supplied to the external loads. Dye is regenerated through accepting the electrons from I^- and the resulting I_3^- is reduced at the counter electrode by taking the electrons contributed by the external circuit. All four units of the DSSCs receive constant and continuing research attention. This work focuses on the structure of the TiO_2 porous film. As is common practice in this area, TiO_2 NPs of 15–30 nm are pasted and cast on a transparent conducting glass, followed by calcination to acquire the porosity and anatase crystallinity of the TiO_2 film.

The connection between neighboring TiO_2 NPs plays an important role in achieving high light-to-electricity conversion efficiencies for DSSCs. For randomly packed TiO_2 NPs films, the transport of electrons has been shown to be restricted

by the residence time of the electrons in traps [11–13], the morphology of the particle network [14], and the interconnection of NPs [15]. Efficient electron transport is thus one of the keys to improving the efficiency of DSSCs.

In light of this, several attempts have been made to improve the efficiency of electron transport by using one-dimensional (1D) nanostructures of TiO_2 as the anode of DSSCs. These 1D nanostructures serve as the electron transport highway to avoid excess amounts of NP contacts existing in the NP packed films. The regular spatial arrangement of the 1D nanostructure array also enhances the ion diffusion at the TiO_2–dye–electrolyte interfaces. Several types of 1D nanostructure array have been investigated for these purposes. These nanostructures, including nanowires, nanorods and nanotubes, were prepared through the use of surfactant templates [16, 17], a hydrothermal process [18, 19], and anodization of titanium foils [20–22].

In addition to these 1D nanostructure arrays, there are other possible alternatives, for example, ordered porous structures with a thin shell. The thin shell of the porous structure plays a similar role as the 1D nanostructures in providing fast electron transport paths. One such example is the inverse opal structure, which is derived from the corresponding synthetic opal structure and is a popular structure for applications in photonic crystals. Because of the development of photonic crystals, a tremendous amount of research effort has been devoted to the fabrication of synthetic opals. One popular way of constructing synthetic opals is through evaporation-assisted assembly of uniform sized colloidal particles, such as polystyrene (PS) and silica spheres, due to the process simplicity, cost effectiveness, and extensibility to large scale production [23–25]. The corresponding inverse opals can then be obtained by filling target materials, here TiO_2, into the void of the synthetic opal through processes such as chemical vapor deposition [26], electrochemical deposition [27] or nanoparticle infiltration [28] and subsequently removing the starting synthetic opal by solvent etching or calcination, leaving behind the inverse opal of the target material.

There are several potential advantages associated with the use of inverse opals as the anode for DSSCs. First, the inverse opal structure is the closest packing of spherical voids arranged in a face-centered cubic (FCC) array, which leads to the highest spherical surfaces per unit volume available for dye adsorption. Second, the ordered and continuous thin shell of the inverse opal structure serves as the fast electron transport paths. Third, the highly ordered structure of the inverse opal reduces the mass transfer resistances of electrolyte transport and dye impregnation within the regularly connected spherical voids and thus results in efficient electrolyte–dye interactions.

The thin shells existing in the inverse opal structure can speed up electron transport because of the geometric confinement and structural regularity effects. Electron transport in 2D thin shells would be faster than in 3D space because of the reduction in degrees of freedom for electron movement. The geometric confinement would force the electron transport to be less diffusive and pointing to more specific directions. The structural regularity of the inverse opal structure helps reduce tortuosity in the electron transport paths, thus favoring electron transport. The regularity of the inverse opal structure offers not only more direct transport paths for electrons but also regular mass transfer channels for liquid electrolytes and dye solutions. The regularity in mass transfer channels makes the transport paths of the liquid phase species less tortuous to speed up their mass transport rate.

In this paper, we propose a novel multi-scale nanostructure of TiO_2 as the anode of DSSCs. The structure is composed of a blocking layer of TiO_2, an inverse opal of TiO_2 possessing spherical voids, interconnected transport channels between neighboring spherical voids, and TiO_2 NPs coated on the spherical surfaces of the voids. The highly ordered TiO_2 inverse opal was fabricated on a blocking layer covered FTO substrate, starting from the self-assembly of PS spheres to form the sacrificial synthetic opal template followed by electrochemical deposition of TiO_2 and calcination to obtain the TiO_2 inverse opal of anatase crystallinity. To acquire sufficient thickness of the inverse opal without detachment from the substrate, a multi-cycle procedure of PS opal deposition and electrochemical TiO_2 infiltration was developed. Finally, the surfaces of the spherical voids were decorated with TiO_2 NPs through $TiCl_4$ treatment to increase the TiO_2 surface area for dye adsorption. The resulting anodes were measured for the conversion efficiency under AM 1.5 illumination. The positive influences of the increase in inverse opal thickness and introduction of NP decoration were observed. The efficiency increased from 2.3 to 3.7% with the increase in thickness from 4 to 12 μm, while the efficiency was further increased to 4% when the NP decoration was performed.

It is worth noting that, although the idea of taking TiO_2 inverse opals as the anode has been adopted on solid-state DSSCs [29, 30], insufficient thickness, less regular structure, and not small enough characteristic structural length of the TiO_2 inverse opal obtained in these previous works resulted in poor conversion efficiency. The present work improved significantly on the aspects of thickness, structural regularity, and functioning TiO_2 surface area, among other factors, to obtain much better conversion efficiency.

2. Experimental details

2.1. Synthesis of PS spheres

Uniform sized PS spheres were prepared using an emulsifier-free emulsion polymerization process [31]. The sphere size was controlled to be around 100 nm by adjusting the concentration of the co-monomer, sodium styrene sulfonate. In a typical synthesis, 0.4 g of sodium styrene sulfonate and 0.25 g of sodium bicarbonate were added into 450 g of deionized water preheated to 75 °C. After stirring for 10 min, 50 g of styrene monomer was added into the solution and the mixture was further stirred for 2 h. The polymerization was then initiated by introducing 0.25 g of initiator, potassium persulfate, into the solution. The reaction proceeded for 24 h. The resulting PS spheres were 100 nm in diameter, and they were used without further purification.

2.2. Treatment of transparent conducting substrate

FTO (Solaronix, 10 Ω/square) glass was used as the transparent conducting substrate. Before use, a thin dense TiO_2 layer was electrochemically deposited onto the FTO glass to serve as a blocking layer. The electrochemical deposition of TiO_2 was carried out from a 50 mM aqueous solution of $TiCl_3$ at pH 2.8 (titrated by 2 M NaOH) by galvanostatic oxidation at 0 V (versus the SCE) in a three-electrode cell using Pt as the counter electrode and a saturated calomel electrode (SCE) as the reference electrode.

2.3. Assembly of PS spheres on the substrate

PS spheres were self-assembled on the transparent conducting substrate by using an evaporation-assisted vertical deposition process. Typically, the substrate was immersed vertically into a PS suspension of 0.125 wt% of 60 °C. With evaporation of water, the PS spheres self-assemble into a face-centered cubic array, commonly referred to as synthetic opal, on the substrate surface.

2.4. Fabrication of TiO_2 inverse opal

TiO_2 was electrochemically deposited into the voids of the PS opal formed on the blocking layer covered FTO substrate through the same procedure described for the blocking layer preparation. The PS opal was then removed by calcination in air or O_2 atmosphere at 450 °C for 2 h. A heating rate of 2 °C min^{-1} was used to reach the calcination temperature from room temperature. The resulting TiO_2 inverse opal was then immersed in 0.1 or 0.4 M ethanolic $TiCl_4$ solution for 30 min at 60 °C. After rinsing with deionized water, the electrode was calcined in air or O_2 atmosphere again for 30 min to obtain the TiO_2 NP decoration.

2.5. Cell assembly

The TiO_2 inverse opal built on the conducting substrate was partially scraped off to form an active area of 0.2 cm^2 before dye impregnation. The sample was preheated at 90 °C for 30 min to remove the water adsorbed on the TiO_2 surfaces and then quickly immersed in a 0.3 mM acetonitrile/tert-butyl alcohol (1:1) solution containing ruthenium dye, cis-bis(isothiocyanato)bis(2, 2′-bipyridyl-4, 4′-dicarboxylato)-ruthenium(II)bis-tetrabutylammonium (N719), for 12 h, followed by rinsing in absolute ethanol (99.8%) to remove unabsorbed dye. A 100 nm thick layer of platinum was coated onto an ITO glass (15 Ω/square) by thermal evaporation under vacuum (10^{-6} Torr) at a deposition rate of 1 Å/1 s to serve as the counter electrode. The dye loaded anode and Pt counter electrode were sealed together with a sealing material, SX1170 (Solaronix), around the TiO_2 active area. The electrolyte, containing 0.6 M 1-propyl-2,3-dimethylimidazolium iodide (DMPII), 0.1 M lithium iodide, 0.05 M iodine, and 0.5 M 4-tert-butylpyridine (TBP) in 3-methoxypropionitrile (MPN), was then introduced into the cell.

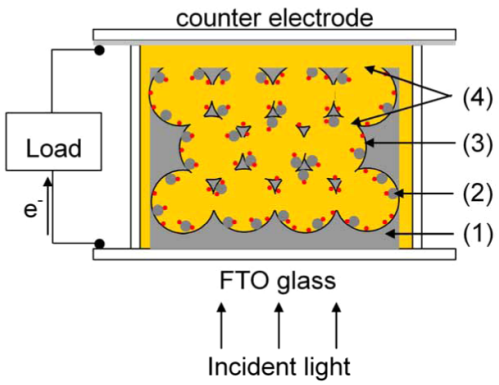

Figure 1. Schematic illustration of the proposed multi-scale nanostructure of TiO_2 used as the anode in DSSCs. (1) TiO_2 blocking layer, (2) TiO_2 NPs, (3) TiO_2 inverse opal backbone, and (4) interconnected transport channels for dye (red dots) impregnation and electrolyte (yellow part) transfer.

2.6. Characterizations

Field emission scanning electron microscope (FE-SEM) images were obtained on a JEOL JSM-6700 microscope operated at 3 kV. Transmission electron microscope (TEM) and selected area electron diffraction (SAED) pattern studies were performed on a JEOL JEM-2010 microscope operated at 200 kV. The TiO_2 inverse opal was scraped off, redispersed in ethanol and dripped onto a carbon-coated copper grid for TEM characterizations. X-ray diffraction (XRD) spectra were recorded on an MAC Science MXP18 x-ray diffractometer ($\lambda = 1.540\,56$ Å). The current density–voltage (J–V) curve was measured with a source meter (Keithley, model 2400) under illumination by a Newport solar simulator (AM 1.5, 100 mW cm^{-2}) with a scan rate of 10 mV s^{-1}.

3. Results and discussion

Figure 1 illustrates the proposed multi-scale TiO_2 nanostructure. We first deposit a thin, dense TiO_2 layer on the FTO glass to serve as the electron blocking layer. The TiO_2 inverse opal is then constructed on top of the blocking layer as the main structure of the anode. The spherical surfaces of the voids of the inverse opal are further decorated with TiO_2 NPs to increase the contact area between TiO_2 and dye. This completes the construction of the multi-scale TiO_2 nanostructure, which involves a blocking layer of 90 nm thickness, an inverse opal of 100 nm voids, transport channels of 30–50 nm between neighboring voids, and NPs of 10–15 nm. The electrons, once generated from the excited dyes, can be transported toward the FTO glass through the regular, continuous pathways provided by the highly ordered inverse opal thin shell. The transport channels between neighboring voids are arranged regularly in space to ensure the complete penetration of electrolyte and dye into the void and reduce the mass transfer resistances of electrolytes in and out of the porous structure. This TiO_2 anode is then integrated with the Pt counter electrode to complete the assembly of a DSSC.

It has been shown that a dense layer of TiO_2 placed between the FTO substrate and the active TiO_2 structure can

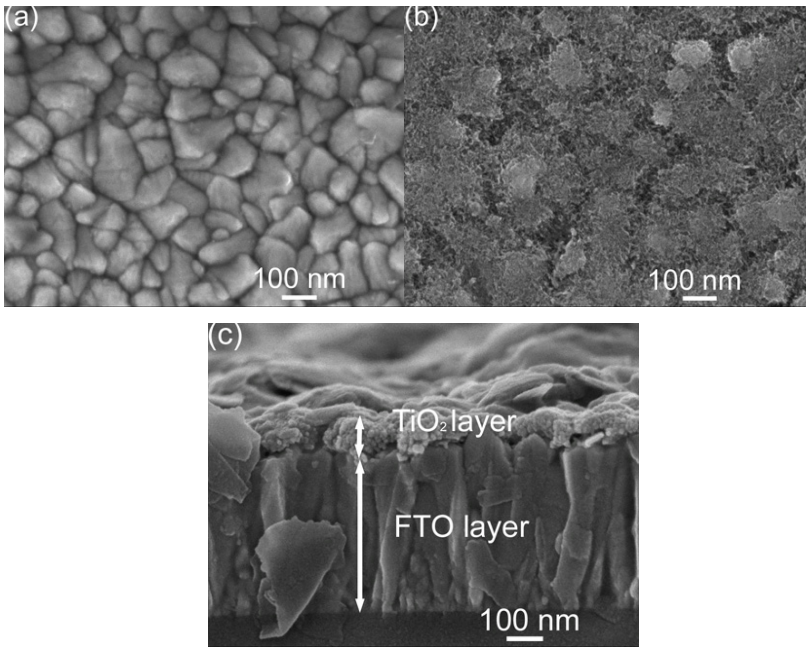

Figure 2. Top view SEM images of (a) a plain FTO substrate and (b) an FTO substrate coated with a TiO_2 blocking layer. (c) Side view SEM image of the FTO substrate with a TiO_2 blocking layer coated on top of it. The thickness of the TiO_2 blocking layer is around 90 nm.

inhibit the transfer of excited electrons back to the electrolyte phase and thus benefit the conversion efficiency [32–34]. For the TiO_2 blocking layer to be effective, a minimum layer thickness is required [34]. In this study, the blocking layer of 90 nm was obtained through electrochemical deposition. With electrochemical deposition, the layer thickness can be easily controlled by altering the deposition time. Figures 2(a) and (b) show the nanostructure of the top surface of the FTO substrate before and after the electrochemical deposition of the TiO_2 blocking layer, respectively. Apparent morphological changes of the substrate top surface were observed, implying the successful deposition of the TiO_2 film onto the FTO substrate. The layer thickness was determined to be around 90 nm from the side view SEM image of the substrate as shown in figure 2(c).

Before an inverse opal structure can be constructed, we need a sacrificial opal structure to serve as the starting template. Here, uniform sized PS spheres were used for this purpose through the evaporation-assisted self-assembly. There is, however, one technical challenge to be overcome first. The adhesion between the PS opal and the TiO_2 coated FTO substrate is rather poor, and thus thick PS opals are difficult to obtain without de-attachment from the substrate. Here, we developed a multi-cycle procedure to solve this problem. As illustrated in figure 3, we start with the construction of a thin opal layer. The infiltration of TiO_2 into the void space of the thin opal is performed next. The adhesion of the deposited TiO_2 to the TiO_2 blocking layer is excellent, and it can sustain the subsequent addition of thicker opal structures and accompanying infiltration operations. The desired thickness of the final TiO_2 inverse opal can be easily tailored by repeating the PS deposition–TiO_2 infiltration cycle.

Besides the advantage of increasing the thickness of the functioning inverse opal structure, the present multi-

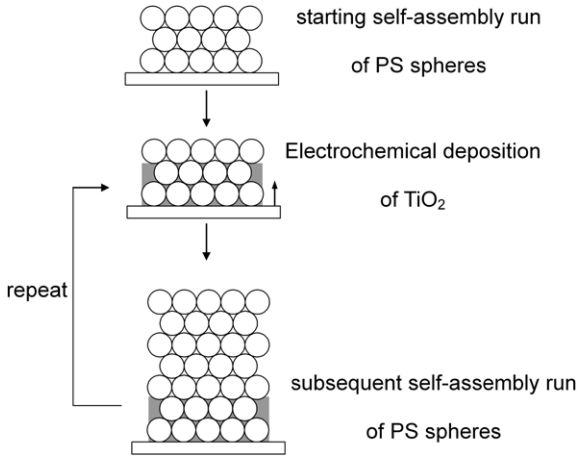

Figure 3. Illustration of the multi-cycle procedure.

cycle procedure can offer another potential advantage. It has been theoretically predicted that multi-layer photonic crystals of varying lattice constants can improve the light harvesting efficiency of DSSCs through optical absorption amplification [35, 36]. This multi-layer photonic crystal concept may be realized with the present multi-cycle procedure.

To obtain a firm starting PS opal layer, the particle concentration of the PS suspension needs to be carefully controlled to avoid potential de-attachment of the resulting PS opal from the substrate. A particle concentration of 0.125 wt% was found to be proper for the present study. The subsequent TiO_2 infiltration step also needs care to avoid overgrowth. Overgrowth of TiO_2 will make the subsequent run of PS assembly more difficult, and more importantly will block the

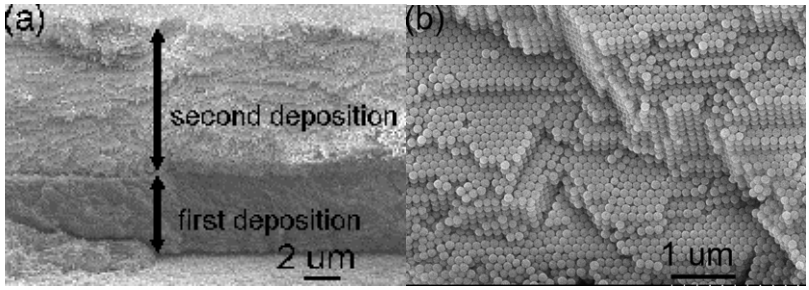

Figure 4. (a) A two-layer PS opal constructed from the multi-cycle procedure. The first layer was infiltrated with TiO_2. (b) A closer view of a fractured part of the PS opal of the second deposition, revealing the FCC close packing of PS spheres.

transport channels between interfacial voids. The subsequent PS opal can be constructed in a much larger thickness than the starting PS opal layer since the first TiO_2 infiltration layer provides a firm footing and the adhesion between the two neighboring PS layers is strong. By repeating the PS deposition–TiO_2 infiltration cycle, one can generate PS opals of large thicknesses. With the present approach, we have successfully obtained a PS opal 25 μm in thickness, and the resulting PS opal adhered well onto the TiO_2 covered FTO substrate. A typical TiO_2 infiltrated PS opal obtained in this study is shown in figure 4(a). The thickness of the PS opal obtained increases from 4 μm after the first run deposition to 8 μm after the second run deposition, confirming the feasibility of the proposed approach. Figure 4(b) shows the typical face-centered cubic close packing of PS spheres in the resulting PS opal. The (111) and (100) crystalline planes of the FCC array are clearly identified in figure 4(b), in which the PS spheres are hexagonally arranged on the (111) plane and squarely packed on the (100) plane.

The TiO_2 infiltrated PS opal was calcined in an oxygen containing atmosphere to remove the PS template and also to acquire the anatase crystallinity necessary for better conversion efficiency of the DSSC. The resulting TiO_2 inverse opal was further treated with 0.1 M ethanolic $TiCl_4$ to introduce TiO_2 NPs into the inverse opal structure to increase the active TiO_2 surface area. The $TiCl_4$ post-treatment, in addition to providing extra TiO_2 surface area, has been proven to also enhance the light absorption and dye adsorption of the anode, benefiting the conversion efficiency [21, 37, 38]. Although the unique optical property of inverse opal, the photonic band-gap, reflected light within the band-gap range, the prepared TiO_2 inverse opal here has a theoretical band-gap position below 250 nm, which is far away from the peak absorption of dye located at 370 and 500 nm. Furthermore, the energy of the light within the photonic band-gap of prepared inverse opal has reached the electronic band-gap of TiO_2 and consequently disturbed the optical properties by absorption. On the other hand, titania inverse opals of band-gap positions located in the visible regime have been used to enhance light scattering within DSSC cells by coupling the inverse opals to conventional TiO_2 nanoparticle films [39]. In the present work, titania inverse opals play the role of the main porous TiO_2 structure instead of a light scattering enhancing layer. The prepared $TiCl_4$ treated inverse opal appeared white as traditional nanoparticle based DSSCs, and no obvious reflection (i.e., >2%) was measured.

The morphology of the TiO_2 inverse opal with and without the TiO_2 NP decoration was characterized with an SEM and a TEM. The successful introduction of the TiO_2 NPs onto the spherical surfaces of the voids was confirmed from both SEM and TEM images. Figure 5(a) shows the TiO_2 inverse opal with good periodicity and smooth surfaces before the TiO_2 NP decoration. The highly ordered and continuous TiO_2 backbone serves as the pathway for fast electron transport within the structure, and the regularly arranged transport channels of 30–50 nm can ease the transfer of dye and electrolyte in the liquid phase. Once the TiO_2 inverse opal was treated with $TiCl_4$, the precursor of TiO_2, the adsorbed $TiCl_4$ was oxidized to form TiO_2 NPs with calcinations in air or oxygen atmosphere. As shown in figure 5(b), the apparent roughness of the spherical surfaces of the voids indicates a successful introduction of TiO_2 NPs. Although this post-treatment showed a positive influence on the conversion efficiency, the concentration of the ethanolic $TiCl_4$ needs careful control. If the concentration of $TiCl_4$ is too high, the transport channels of the inverse opal may be blocked by the large amount of TiO_2 NPs formed around the transport channel, reducing the surface available for and obstructing the penetration of dye and electrolyte. Consequently, the conversion efficiency decreases. As an example, the morphology of the inverse opal treated with 0.4 M ethanolic $TiCl_4$ is shown in figure 5(c). Evidently, most transport channels were clogged. Figure 5(d) shows the side view of a TiO_2 inverse opal with a thickness of 12 μm, a typical thickness for the anode of DSSCs [40].

The morphology of the TiO_2 inverse opal was further characterized with a TEM and HRTEM. The TEM image shown in figure 6(a) further confirms the successful decoration of the inverse opal with TiO_2 NPs. TiO_2 NPs of 10–15 nm in diameter were attached to the backbone of the TiO_2 inverse opal, leaving transport channel openings of 30–50 nm for dye and electrolyte transfer. The high resolution lattice resolved image shown in figure 6(b) was taken at the junction of three spherical voids. As shown in figure 6(b), the TiO_2 NPs were well crystallized and well connected. The inset of figure 6(b) shows the lattice fringes of a TiO_2 nanocrystal; the spacing between two neighboring crystalline planes is 0.35 nm, in good agreement with the d-spacing of the (101) planes of anatase TiO_2. The corresponding selected area electron diffraction pattern of the TiO_2 inverse opal is shown in figure 6(c). The ring pattern can be indexed to the anatase crystalline phase of TiO_2. Note that anatase phase is preferred for DSSC

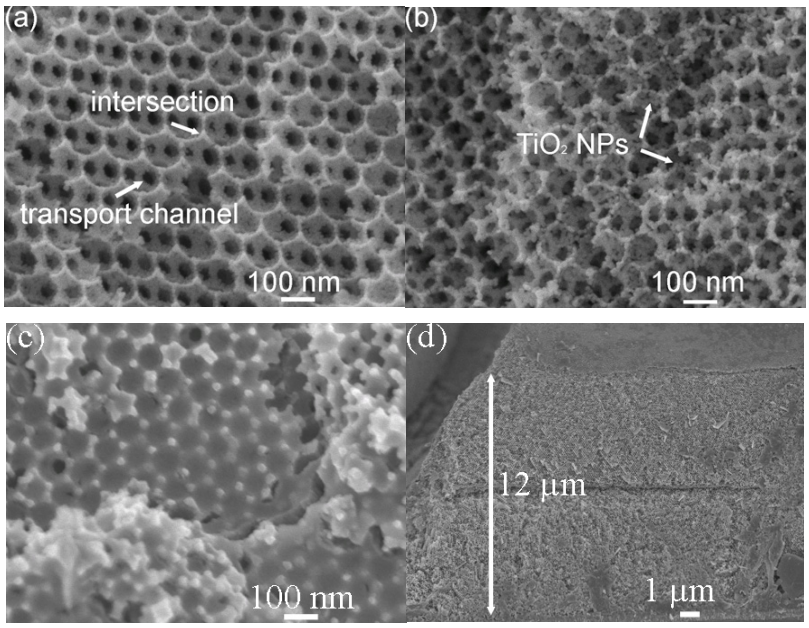

Figure 5. SEM images of the TiO_2 inverse opal (a) before and (b) after the $TiCl_4$ post-treatment. (c) The side view SEM image of the TiO_2 inverse opal after a $TiCl_4$ treatment of high concentrations. (d) The side view SEM image of the TiO_2 inverse opal.

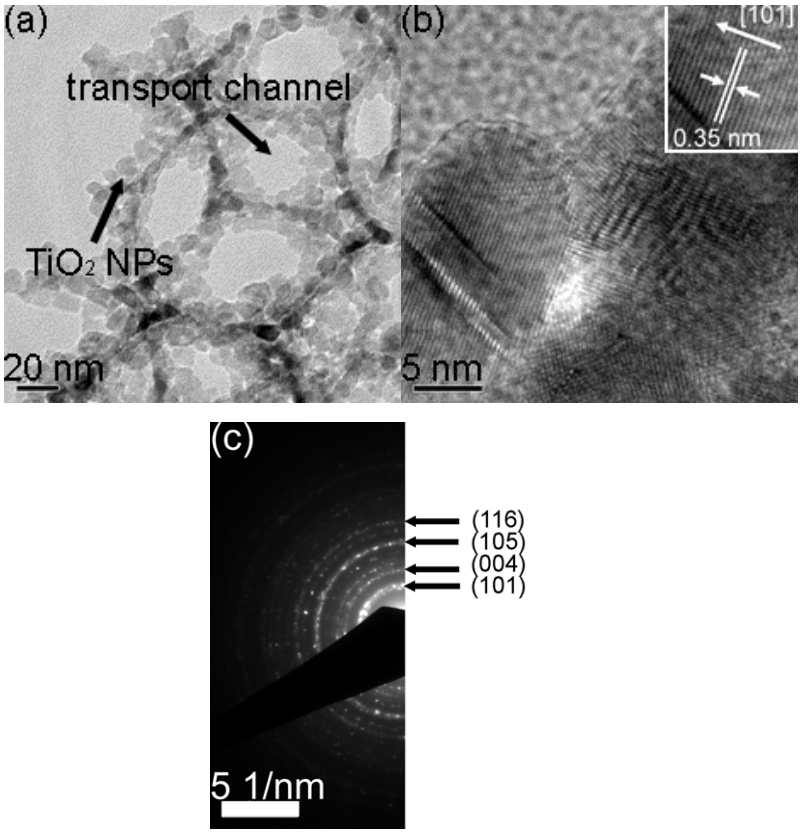

Figure 6. (a) TEM image of the TiO_2 NP decorated TiO_2 inverse opal, (b) HRTEM image taken at a junction of three spherical voids, (c) selected area electron diffraction pattern of the TiO_2 inverse opal, indicating the anatase crystalline phase.

applications. We further compared the crystallinity of the TiO_2 inverse opal calcined in air and O_2 with XRD characterizations. Curve (a) of figure 7 shows the typical diffraction pattern of a plain FTO substrate after calcination. After the TiO_2 was infiltrated into the voids of the PS opal (curve (b)), no extra diffraction peaks attributable to TiO_2 were observed, indicating that the as-infiltrated TiO_2 was amorphous. Once the samples were calcined in air or O_2 atmosphere, diffraction peaks of

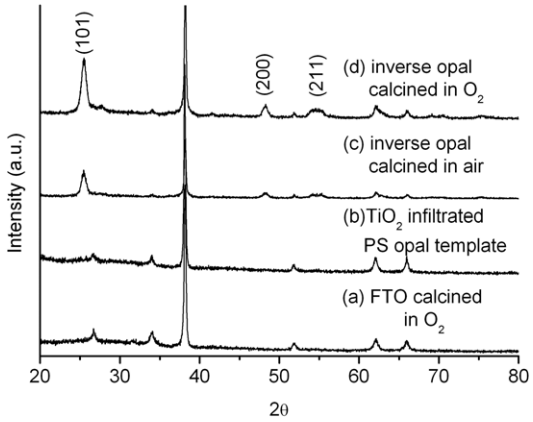

Figure 7. XRD spectra of samples treated under various conditions. The extra diffraction peaks of curves (c) and (d) can be indexed to the anatase phase of TiO_2.

anatase TiO_2 appeared. If examined closely, the sample calcined in O_2 atmosphere gave stronger diffraction peaks (curve (d)) as compared with those from calcination in air (curve (c)), implying that better crystallinity was obtained with calcination performed in O_2 atmosphere. Since the crystallinity of TiO_2 benefits the injection and transport of electrons within the structure [41, 42], better crystallinity is desired to achieve higher conversion efficiency.

Since electron-transfer kinetics significantly influence the conversion efficiency of DSSCs, the electron lifetime (denoted as τ_n) as a function of open-circuit potential (V_{oc}) for the present multi-scale TiO_2 nanostructure was studied with a V_{oc} decay technique [43, 44]. The same investigation was also performed for the DSSCs constructed by casting TiO_2 NPs of about 20 nm on FTO for comparison. The NP film was 13 μm in thickness. The value of V_{oc} was recorded against the measuring time when the illumination state was changed from 100% AM 1.5 to dark. The electron lifetime τ_n can be related to the V_{oc} decay as

$$\tau_n = -\frac{k_B T}{e}\left(\frac{dV_{oc}}{dt}\right)^{-1}. \quad (1)$$

Here, $k_B T$ is the thermal energy, e is the positive elementary charge, and dV_{oc}/dt is the time derivative of V_{oc}. This formula is generally appropriate for the V_{oc} decay observed in DSSCs [42]. The resulting V_{oc} decay and corresponding lifetime derived from equation (1) for the present multi-scale TiO_2 nanostructure and TiO_2 NP film are plotted in figure 8. Evidently, the DSSC constructed from the TiO_2 NP casting shows a much quicker decay in V_{oc} and thus a much shorter electron lifetime, revealing the advantage of the present multi-scale TiO_2 nanostructure in providing an environment of superior electron recombination characteristic [21].

The fabricated multi-scale TiO_2 nanostructure was assembled into a DSSC, from which the conversion efficiency was measured. The current density–voltage (J–V) curves, shown in figure 9, were recorded with a source meter at the measurement conditions of 0.2 cm^2 active area under 100% simulated sunlight AM 1.5 illumination. The test cell with a TiO_2 inverse opal thickness of 4 μm (curve (a)) gives a short-circuit current density (J_{sc}) of 5.5 mA cm^{-2}, a V_{oc} of 0.72 V, and a fill factor of 0.58 to produce an overall conversion

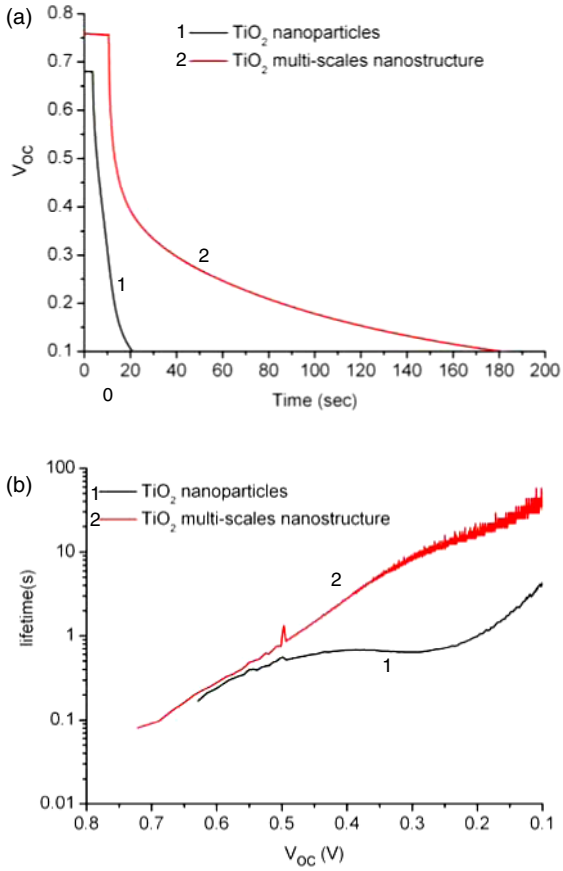

Figure 8. (a) V_{oc} decay and (b) electron lifetime of the DSSCs constructed from the multi-scale TiO_2 nanostructure and TiO_2 NP film when the illumination state was changed from 100% AM 1.5 to dark.

(This figure is in colour only in the electronic version)

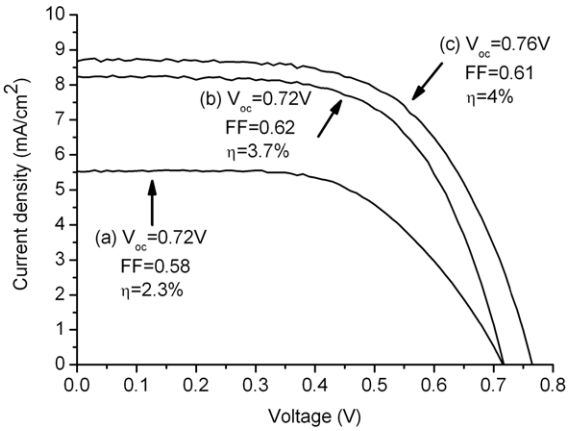

Figure 9. J–V curves of the multi-scale TiO_2 nanostructure based DSSCs. (a) 4 μm inverse opal without $TiCl_4$ treatment, (b) 12 μm inverse opal without $TiCl_4$ treatment, and (c) 12 μm inverse opal with $TiCl_4$ treatment.

efficiency of 2.3%. If the thickness of the TiO_2 inverse opal was increased to 12 μm (curve (b)), a J_{sc} of 8.2 mA cm^{-2}, a V_{oc} of 0.72 V, and a fill factor of 0.62 were obtained, and the conversion efficiency rose to 3.7%. If the TiO_2 inverse opal was subjected to the $TiCl_4$ treatment (curve (c)), both the J_{sc} and V_{oc} were further improved to reach 8.7 mA cm^{-2} and 0.76 V, respectively, yielding an even higher conversion efficiency of 4%, an 8% improvement from the untreated TiO_2 inverse opal. For the present case, the photocurrent density was already high enough for the untreated inverse opal and thus an 8% improvement should be considered reasonable [37, 38].

4. Conclusion

A highly ordered multi-scale nanostructure of TiO_2 with controllable thickness was successfully fabricated to serve as the anode of DSSCs. The structure is composed of a TiO_2 blocking layer of 90 nm thickness, a TiO_2 inverse opal possessing spherical voids of 100 nm in diameter, regularly arranged transport channels of 30–50 nm in diameter between neighboring spherical voids, and TiO_2 NPs of 10–15 nm in diameter coated on the spherical surfaces of the voids. As compared with traditional TiO_2 NP based DSSCs, the present highly ordered multi-scale nanostructure of TiO_2 showed longer electron lifetime, indicating that a superior electron recombination characteristic was achieved in this structure. A conversion efficiency of 4% with a fill factor of 0.61 has been achieved under AM 1.5 illumination by using this structure as the anode of the DSSC. The proposed multi-scale TiO_2 nanostructure, although offering many advantages, still suffers a main drawback of not high enough surface area available for dye adsorption and subsequent optical–electric conversion, as compared with conventional DSSC cells. Further investigation needs to be done on this issue.

Acknowledgment

This work was financially supported by the National Science Council of the Republic of China (Taiwan) under grant NSC-95-2221-E-007-194.

References

[1] O'Regan B and Grätzel M 1991 *Nature* **353** 737
[2] Nazeeruddin M K, Kay A, Rodicio I, Baker R H, Müller E, Liska P, Vlachopoulos N and Grätzel M 1993 *J. Am. Chem. Soc.* **115** 6382
[3] Bach U, Lupo D, Comte P, Moser J E, Weissortel F, Salbeck J, Spreitzer H and Grätzel M 1998 *Nature* **395** 583
[4] Papageorgious N, Barbe C and Grätzel M 1998 *J. Phys. Chem.* B **102** 4156
[5] Grätzel M 2001 *Nature* **414** 338
[6] Palomares E, Clifford J N, Haque S A, Lutz T and Durrant J R 2003 *J. Am. Chem. Soc.* **125** 475
[7] Grätzel M 2004 *J. Photochem. Photobiol.* A **164** 3
[8] Hu L H *et al* 2007 *J. Phys. Chem.* B **111** 358
[9] Cao F, Oskam G, Meyer G J and Searson P C 1996 *J. Phys. Chem.* **100** 17021
[10] Dloczik L, Ileperuma O, Lauermann I, Peter L M, Ponomarev E A, Redmond G, Shaw N J and Uhlendorf I 1997 *J. Phys. Chem.* B **101** 10281
[11] Schlichthoŕl G, Park N G and Frank A J 1999 *J. Phys. Chem.* B **103** 782
[12] van de Lagemaat J and Frank A J 2001 *J. Phys. Chem.* B **105** 11194
[13] Benkstein K D, Kopidakis N, van de Lagemaat J and Frank A J 2003 *J. Phys. Chem.* B **107** 7759
[14] Law M, Greene L E, Johnson J C, Saykally R and Yang P D 2005 *Nat. Mater.* **4** 455
[15] Adachi M, Murata Y, Takao J, Jiu J T, Sakamoto M and Wang F M 2004 *J. Am. Chem. Soc.* **126** 14943
[16] Adachi M, Murata Y, Okada I and Yoshikawa S 2003 *J. Electrochem. Soc.* **150** G488
[17] Ngamsinlapasathian S, Sakulkhaemaruethai S, Pavasupree S, Kitiyanan A, Sreethawong T, Suzuki Y and Yoshikawa S 2004 *J. Photochem. Photobiol.* A **164** 145
[18] Wei M D, Konishi Y, Zhou H S, Sugihara H and Arakawa H 2006 *J. Electrochem. Soc.* **153** A1232
[19] Jiu J T, Isoda S, Wang F M and Adachi M 2006 *J. Phys. Chem.* B **110** 2087
[20] Paulose M, Shankar K, Varghese O K, Mor G K, Hardin B and Grimes C A 2006 *Nanotechnology* **17** 1446
[21] Mor G K, Shankar K, Paulose M, Varghese O K and Grimes C A 2006 *Nano Lett.* **6** 215
[22] Zhu K, Neale N R, Miedaner A and Frank A J 2007 *Nano Lett.* **7** 69
[23] Lin Y R, Kuo C Y and Lu S Y 2004 *Appl. Phys.* A **79** 1741
[24] Hsiao S Y, Wong D S H and Lu S Y 2005 *J. Am. Ceram. Soc.* **88** 974
[25] Kuo C Y, Lu S Y, Chen S, Bernards M and Jiang S 2007 *Sensors Actuators* B **124** 452
[26] Miguez H *et al* 2001 *Adv. Mater.* **13** 1634
[27] Bartlett P N, Ghanem M A, El Hallag I S, de Groot P and Zhukov A 2003 *J. Mater. Chem.* **13** 2596
[28] Wang D Y, Salgueirino-Maceira V, Liz-Marzan L W and Caruso F 2002 *Adv. Mater.* **14** 908
[29] Somani P R, Dionigi C, Murgia M, Palles D, Nozar P and Ruani G 2005 *Sol. Energy Mater. Sol. Cells* **87** 513
[30] Huisman C L, Schoonman J and Goossens A 2005 *Sol. Energy Mater. Sol. Cells* **85** 115
[31] Kim J H, Chainey M, Elaasser M S and Vanderhoff J W 1989 *J. Polym. Sci.* A **27** 3187
[32] Cameron P J and Peter L M 2003 *J. Phys. Chem.* B **107** 14394
[33] Xia J, Masaki N, Jiang K and Yanagida S 2006 *J. Phys. Chem.* B **110** 25222
[34] Hart J N, Menzies D, Cheng Y B, Simon G P and Spiccia L 2006 *C. R. Chim.* **9** 622
[35] Mihi A and Míguez H 2005 *J. Phys. Chem.* B **109** 15968
[36] Mihi A, Lopez-Alcaraz F J and Míguez H 2006 *Appl. Phys. Lett.* **88** 193110
[37] Sommeling P M, O'Regan B, Haswell R R, Smit H J P, Bakker N J, Smits J J T, Kroon J M and van Roosmalen J A M 2006 *J. Phys. Chem.* B **110** 19191
[38] Ito S *et al* 2005 *Chem. Commun.* **34** 4351
[39] Halaoui L I, Abrams N M and Mallouk T E 2005 *J. Phys. Chem.* B **109** 6334
[40] Grätzel M 2005 *Inorg. Chem.* **44** 6841
[41] Byun H Y, Vittal R, Kim D Y and Kim K J 2004 *Langmuir* **20** 6853
[42] Hou K, Tian B Z, Li F Y, Bian Z Q, Zhao D Y and Huang C H 2005 *J. Mater. Chem.* **15** 2414
[43] Zaban A, Greenshetin M and Bisquert J 2003 *ChemPhysChem* **4** 859
[44] Bisquert J, Zaban A, Greenshetin M and Mora-Sero I 2004 *J. Am. Chem. Soc.* **126** 13550